HHS Public Access

Author manuscript

Nat Cell Biol. Author manuscript; available in PMC 2010 August 01.

Published in final edited form as:

Nat Cell Biol. 2010 February ; 12(2): 193–199. doi:10.1038/ncb2019.

Regulation of NF-κB inhibitor IκBα and viral replication by a KSHV microRNA

Xiufen Lei[1,2,7], **Zhiqiang Bai**[1,2,3,4,7], **Fengchun Ye**[1,2], **Jianping Xie**[1,2], **Chan-Gil Kim**[1,5], **Yufei Huang**[1,6], and **Shou-Jiang Gao**[1,2,3,4,8]

[1]Tumor Virology Program, Greehey Children's Cancer Research Institute, The University of Texas Health Science Center at San Antonio, San Antonio, Texas 78229, USA

[2]Department of Pediatrics, Microbiology and Immunology, Medicine, and Molecular Medicine, and Cancer Therapy and Research Center, The University of Texas Health Science Center at San Antonio, San Antonio, Texas 78229, USA

[3]Tumor Virology Group, Wuhan Institute of Virology, Chinese Academy of Sciences, Wuhan, Hubei, China 430071

[4]Graduate University of the Chinese Academy of Sciences, Beijing, China 100039

[5]Department of Biotechnology, Konkuk University, Chungju 380-701, Korea

[6]Department of Electrical and Computer Engineering, The University of Texas at San Antonio, San Antonio, Texas 78249, USA

Abstract

Kaposi's sarcoma-associated herpesvirus (KSHV) is causally linked to several acquired immune deficiency syndrome related malignancies including Kaposi's sarcoma (KS), primary effusion lymphoma (PEL), and a subset of multicentric Castleman's disease1. Control of viral lytic replication is essential for KSHV latency, evasion of host immune system, and induction of tumors1. Here, we show that deletion of a cluster of 14 microRNAs (miRs) from KSHV genome significantly enhances viral lytic replication as a result of reduced NF-κB activity. The miR cluster regulates NF-κB pathway by reducing the expression of IκBα protein, an inhibitor of the NF-κB complexes. Computational and miR seed mutagenesis analyses identify KSHV miR-K1 that

[8]Correspondence should be addressed to S.-J.G. (gaos@uthscsa.edu).
[7]These authors contributed equally to this work.

AUTHOR CONTRIBUTIONS

Data of genetics, viral replication, NF-κB-related analysis, and microRNA suppressor were obtained by X.F.L (Fig. 1–4, Supplementary Information, Fig. S1-S3, S5, S6, S8); bioinformatics, mutagenesis of the miR target, and part of the genetics and viral replication were conducted by Z.Q.B. (Fig. 2–3, Supplementary Information, Fig. S1, S4, S7, S8); EMSA was conducted by X.P.X. (Fig. 2); F.C.Y. contributed to the viral genetics and Northern-blotting (Fig. 4, Supplementary Information, Fig. S1). C.G.K. contributed to target identification (Supplementary Information, Fig. S7). Y.F.H. contributed to bioinformatics (Fig. 3). S.J.G. direct, design and analyze all the experiments and data. Manuscript was written by X.F.L. and S.J.G.

COMPETING FINANCIAL INTERESTS

The authors declare no competing financial interests.

SUPPLEMENTARY INFORMATION

Supplementary Information is linked to the online version of the paper.

directly mediates IκBα ?protein level by targeting the 3'UTR of its transcript. Expression of miR-K1 is sufficient to rescue the NF-κB activity and inhibit viral lytic replication while inhibition of miR-K1 in KSHV-infected PEL cells has the opposite effects. Thus, KSHV encodes a miR to control viral replication by activating NF-κB pathway. These results illustrate an important role for KSHV miRs in regulating viral latency and lytic replication by manipulating a host survival pathway.

Keywords

KSHV; microRNA; viral latency and replication; NF-κB; reverse genetics

KSHV encodes 17 miRs, derived from 12 pre-miRs, with largely unknown functions2–5. These miRs are located in the latent genomic locus and expressed during viral latency and in KS tumors2–6. Several KSHV miRs target cellular genes, and thus might play roles in the pathogenesis of KSHV-induced malignancies7–12. However, their roles in viral infection and replication remain unclear.

To determine the function of KSHV miRs in viral lifecycle, we generated a viral mutant, ΔmiRs, with a cluster of 14 miRs (except miR-K10a/b and -K12) deleted and its revertant ΔmiRs_rt (Supplementary Information, Fig. S1). The recombinant viruses were reconstituted in 293T cells, which can be efficiently transfected with large viral DNA genomes, support KSHV persistent infection and replication, and are the only cell type used successfully in conjunction with the KSHV genetic system so far13,14. ΔmiRs cells had no difference in morphology, latent nuclear antigen (LANA) staining pattern, and genome copy number per cell from wild-type virus (WT) cells (Supplementary Information, Fig. S2a–c). Quantitative real-time reverse transcription PCR (RT-qPCR) confirmed the deletion of the miR cluster (Supplementary Information, Fig. S2d). WT and ΔmiRs cells had similar expression levels of latent genes vFLIP and vCyclin in uninduced cells and cells induced with 12-*O*-tetradecanoyl-phorbol-13-acetate and sodium butyrate (T/B) for viral lytic replication (Fig. 1a, first panel). The expression of latent gene LANA was also unchanged in uninduced cells following the miR cluster deletion but was marginally higher in WT than ΔmiRs cells following lytic induction (Fig. 1a, first panel). Immunofluorescence staining showed that WT and ΔmiRs cells had similar expression levels of LANA protein (Supplementary Information, Fig. S2b). In contrast, the expression level of replication and transcription activator (RTA), which activates viral lytic replication, was 4.2-fold higher in ΔmiRs cells than WT cells (Fig. 1a, second panel). While RTA level in WT cells was increased by 3.2-fold following lytic induction, it remained higher in ΔmiRs cells by 2.3-fold. Similar results were observed with KSHV late lytic protein major capsid protein (MCP) (Fig. 1a, third panel). Examination of expression kinetics showed that ΔmiRs cells had significantly higher expression levels of both RTA and MCP throughout the entire lytic induction period (Fig. 1b, c). In addition, the RTA promoter activity was 1.6- and 2.2-fold higher in uninduced and T/B-induced ΔmiRs cells than those of WT cells, respectively (Fig. 1d). Uninduced and T/B-induced ΔmiRs cells also had 3.1- and 4.6-fold more cells stained positive for early viral lytic protein ORF59 than WT cells had, respectively (Fig. 1e). Consistent with these results, ΔmiRs cells produced 2.4-fold more viral particles than WT

cells did following lytic induction (Fig. 1f). This enhanced effect on viral lytic replication following the deletion of miR cluster was specific because viral replication in ΔmiRs_rt cells was reverted to WT cells as reflected by the RTA and MCP expression levels (Fig. 1g). Furthermore, stable expression of the miR cluster in ΔmiRs cells, which resulted in the expression of miRs at levels similar to those of WT cells (Supplementary Information, Fig. S3a), reduced the RTA level by 50% and 41% in uninduced and T/B-induced cells, respectively (Fig. 1h), indicating that the cluster could function in trans. Similar results were observed with MCP. Together, these results indicated that the miR cluster inhibited the expression of viral lytic genes in latent cells, and in cells induced for viral lytic replication.

In a previous study15, computational analysis has predicted several putative targeting sites for KSHV miR-K6 in the 3'UTRs of RTA and ZTA, which shared multiple polycistronic transcripts with the same 3'UTR sequences16. However, we failed to detect any effects of KSHV miRs on these transcripts in 3'UTR reporter assays (Supplementary Information, Fig. S4). Since NF-κB pathway mediates vFLIP inhibition of KSHV lytic replication17, we determined the NF-κB status in ΔmiRs cells. The NF-κB activity was 2.2-fold weaker in ΔmiRs cells than in WT cells in a reporter assay (Fig. 2a). While the NF-κB activity was increased by 3.6-fold in WT cells following T/B induction, it remained 1.8-fold lower in ΔmiRs cells than in WT cells. Consistent with these results, a weaker DNA-protein NF-κB complex band was detected by a gel shift assay in ΔmiRs cells than in WT cells with or without lytic induction (Fig. 2b, c). This band was abolished by specific competitor and supershifted by antibodies to cRel, p50, and p65 but not a control antibody, confirming it as the cRel/p50/p65 NF-κB complex. Furthermore, ΔmiRs cells had substantial less p65 nuclear staining than WT cells (Fig. 2d). While T/B treatment increased p65 nuclear staining in both cell types, those of ΔmiRs cells remained weaker than WT cells. Similar results were also observed with p50 and cRel (Supplementary Information, Fig. S5). Thus, the NF-κB activity was lower in ΔmiRs cells than in WT cells.

We then determined whether the miR cluster could function in trans to regulate NF-κB pathway. Expression of the miR cluster increased the NF-κB activity by 2.1-fold in ΔmiRs cells (Fig. 2e). Although T/B induction increased the NF-κB activity by 4.8-fold in ΔmiRs cells, the miR cluster further increased it by 1.3-fold. Similar results were observed in WT cells though these cells had higher basal NF-κB activity. Expression of the miR cluster alone in uninduced and T/B-induced KSHV-negative cells also increased the NF-κB activity by 2.0- and 1.4-fold, respectively. These results indicated that the miR cluster not only rescued the NF-κB activity in ΔmiRs cells but also itself was sufficient to enhance NF-κB pathway in KSHV-negative cells.

Next, we determined whether NF-κB pathway mediates miR cluster inhibition of viral replication. While the miR cluster suppressed RTA and MCP expression, this effect was reversed by a mutant of the NF-κB complex inhibitor IκBα (NF-κB_DN) in both uninduced and T/B-induced ΔmiRs cells (Fig. 2f, g). NF-κB_DN also increased the expression of RTA and MCP in uninduced and T/B-induced WT and ΔmiRs cells (Supplementary Information, Fig. S6). Thus, we concluded that inhibition of NF-κB pathway enhanced viral lytic replication, and the suppression of viral lytic replication by the miR cluster could be mediated by this pathway.

To identify the target that mediated miR cluster suppression of the NF-κB pathway, we examined the IKK members. Consistent with NF-κB activity (Fig. 2b), the levels of IKKα, IKKβ and IKKγ proteins were higher in WT than in mock cells (Fig. 3a). However, ΔmiR cells also had IKKα, IKKβ and IKKγ protein levels at least comparable to or slightly higher than WT cells (Fig. 3a) albeit their lower NF-κB activity (Fig. 2a–d), indicating that the reduced NF-κB activity in ΔmiR cells was unlikely mediated by the IKK members. Upon T/B induction, the levels of all three proteins were increased but were similar among the three cell types (Fig. 3a), reflecting the stimulating effect of T/B on NF-κB pathway.

We further examined the IκB family members. The level of IκBβ protein was reduced in WT and ΔmiR cells (Fig. 3a), which was consistent with their NF-κB activities (Fig. 2b). Upon T/B induction, the expression of IκBβ protein was further reduced but to comparable levels among the three cell types (Fig. 3a). Constitutive activation of NF-κB activity could increase the levels of IκBα and IκBε through a feedback loop18,19. Indeed, we detected higher IκBε level in both WT and ΔmiR cells than mock cells (Fig. 3a). T/B induction increased the IκBε levels in all three cell types. In contrast to IκBε, the level of IκBα in WT cells was almost the same as the mock cells (Fig. 3a), suggesting that IκBα was suppressed by another factor(s). Deletion of the miR cluster significantly increased IκBα level by 1.51-fold (Fig. 3a). While IκBα levels were reduced in all three cell types following T/B induction, those of ΔmiR cells remained 2.82-fold higher than WT cells. These results indicated that IκBα might be a target of the miR cluster. Indeed, overexpression of the miR cluster in KSHV-infected BCP-1 PEL cells20 reduced IκBα protein level by 63% in uninduced cells and by 73% in T/B induced cells (Fig. 3b). In contrast, under the same condition, the levels of IκBε were only marginally affected by the miR cluster with a reduction of 12% and 11%, respectively (Fig. 3b). Consistent with these results, overexpression of the miR cluster in BCP-1 cells increased NF-κB activity by 3.0- and 1.97-fold in uninduced and T/B-induced cells, respectively (Fig. 3c). To further confirm that IκBα is targeted by the miR cluster, we performed a reporter assay with a IκBα 3'UTR reporter. As shown in (Fig. 3d), the IκBα 3'UTR reporter activity was 2.5-fold higher in ΔmiRs cells than in WT cells. Furthermore, the miR cluster could function in trans in ΔmiRs cells to reduce the reporter activity by as much as 50% (Fig. 3e). Thus, the miR cluster directly targeted the IκBα 3'UTR.

We used the 3'UTR reporter assay to screen the 14 miRs in the cluster, and identified miR-K1 as the miR that targeted IκBα (Supplementary Information, Fig. S7a). As shown in Fig. 3f, miR-K1 reduced the IκBα 3'UTR reporter activity by 30% while both miR-K3 and miR-K11 did not reduce the reporter activity. The miR expression constructs were functional as they suppressed the activities of their sensor reporters containing perfect matching sequences of their respective miRs (Supplementary Information, Fig. S7b). The suppression effect of miR-K1 on IκBα 3'UTR reporter activity increased with its increasing expression level (Fig. 3g; Supplementary Information, Fig. S3b). While deletion of the miR cluster from KSHV genome increased the IκBα 3'UTR reporter activity (Fig. 3d), expression of miR-K1 in ΔmiRs cells, which resulted in miR-K1 expression level similar to that of WT cells (Supplementary Information, Fig. S3c), reversed the trend and reduced the reporter activity by 35% (Fig. 3h).

The interaction of a miR with its target is primarily mediated by a 6- to 7-bp seed sequence at the 5'-end of the miR21. We identified two putative miR-K1 binding sites (S1 and S2) in the IκBα 3'UTR using a miR target prediction software miRanda22 (Fig. 3i). Deletion of both sites from the IκBα 3'UTR totally abolished the inhibitory effect of miR-K1 on the reporter while deletion of any one sites had no detectable effects (Fig. 3j). We further generated reporters with different tandem repeats of the sites. As shown in Fig. 3k, the inhibitory effect of miR-K1 on the reporters increased with the number of the repeats for both sites, reaching 70% and 67% for S1 and S2, respectively, when the reporters containing three repeats of the binding sites were examined. Furthermore, expression of miR-K1 with or without the viral genome significantly reduced the IκBα protein level (Fig. 3l, m; Supplementary Information, Fig. S8). These results clearly indicated that miR-K1 suppressed the IκBα protein by directly targeting its 3'UTR.

The identification of miR-K1 as the miR targeting IκBα indicated that it should regulate NF-κB pathway. Indeed, expression of miR-K1 enhanced NF-κB activity in a dose-dependent fashion (Fig. 4a; Supplementary Information, Fig. S3b). While deletion of the miR cluster reduced the NF-κB activity in KSHV-infected cells (Fig. 2a), expression of miR-K1 was sufficient to rescue the NF-κB activity (Fig. 4b). We further inhibited the function of miR-K1 in KSHV-infected PEL cells using a locked nucleic acids/DNA-mixed oligonucleotide (miR-K1 suppressor), which resulted in the reduction of NF-κB activity by 40% (Fig. 4c). In contrast, we observed minimal effects on the NF-κB activity when suppressor of miR-K3 or -K8 was used (Fig. 4c). As expected, the suppressors reduced the levels of their respective miRs by 82% to 99% (Fig. 4d). Furthermore, miR-K1 suppressor efficiently relieved the suppressive effect of miR-K1 on the activity of its sensor reporter by 1.74-fold (Fig. 4e) and significantly increased the IκBα protein level (Fig. 4f), indicating that it was fully functional.

Finally, we examined the role of miR-K1 in viral lytic replication. While deletion of the miR cluster enhanced viral lytic replication as reflected by increased expression levels of RTA and MCP (Fig. 1a–c), expression of miR-K1 reversed the trend, and reduced the levels of RTA and MCP transcripts by 68% and 46% in uninduced ΔmiRs cells, respectively, and by 65% and 38% in T/B-induced ΔmiRs cells, respectively (Fig. 4g, h). Consistently, miR-K1 suppressor increased the expression of RTA and MCP transcripts in BCP-1 cells by 2.3- and 2.6-fold, respectively, and by 1.5- and 1.4-fold following T/B induction, respectively (Fig. 4i, j). In contrast, we observed minimal effects on the expression of RTA and MCP transcripts when suppressor of miR-K3 or -K8 was used (Fig. 4i, j). The miR-K1 suppressor also increased the expression of lytic protein ORF59 from 2.4% to 8.2% (3.4-fold) in uninduced PEL cells, and from 9.7% to 23% (2.4-fold) following T/B induction (Fig. 4k, l). In Northern hybridization, the miR-K1 suppressor increased the expression of Pan transcript, one of the most abundant viral lytic transcripts, by 3.7- and 3.2-fold, and ORF57 transcript, another viral lytic transcript, by 2.6- and 2.1-fold in uninduced and T/B-induced PEL cells, respectively (Fig. 4m). These results clearly showed that miR-K1 suppressed viral lytic replication.

Several recent studies have shown that miRs of herpesviruses suppress viral replication by directly targeting viral genes15,23–26. Our results show that KSHV encodes a miR to

suppress vial replication by regulating cellular NF-κB pathway. Thus, herpesviruses appear to exploit the miR-mediated suppression pathway as a common mechanism to inhibit viral replication and regulate latency. Both vFLIP and LANA also regulate KSHV replication17,27,28. Hence, KSHV has evolved multiple mechanisms to suppress viral lytic replication to achieve latency (Fig. 4n). The NF-κB pathway regulates innate and adaptive immunity, cell survival, and inflammation29. Oncogenic gammaherpesviruses use multiple strategies to regulate NF-κB activity. Both EBV LMP1 and vFLIP activate NF-κB pathway to promote cell growth and survival, and contribute to viral latency30–32. Our results support a general role of NF-κB pathway in regulating the latency of gammaherpesviruses through two interrelated mechanisms, by inhibiting viral replication and by promoting cell survival (Fig. 4n).

METHODS

Methods and any associated references are available in the online version of the paper.

METHODS

Construction of ΔmiRs and ΔmiRs_rt

The procedures for generating a KSHV mutant with a cluster of 14 KSHV miRs (except miR-K10a/b and -K12) deleted (ΔmiRs) and its revertant (ΔmiRs_rt) were previously described13. The strategy is illustrated in Supplementary Information, Fig. S1a. We first obtained a PCR product with primers 5’TTGAATACAGTTGGGGGTAGTCCGCTGGTATTCCCAGCTGAGGTTGCCTTAGTGTAGGCTGGAGCTGCTTC3’ and 5’GTGCTTCTGTTTGAAGGCGAATAAAACAGGAAGCGGGTTGGACTGGCAGGGTCATATGAATATCCTCCTTAG3’ using plasmid pMS102-Zeocin as a template. This PCR fragment contained a zeocin-resistance cassette (Zeo^R) flanked by loxP sites and 50 bp sequences from the two ends of the miR cluster (genomic position: 122,055 and 119,161). The product was electroporated into *E. coli* strain DH10B containing the wild-type virus BAC36 (WT) and the helper plasmid pGET-rec to facilitate homologous recombination. Zeocin-resistant colonies containing KSHV genomes with the miR cluster deleted and replaced by the Zeo^R were selected. To remove the Zeo^R, a Cre-expression plasmid pCTP-T carrying a tetracycline-resistance gene (Tc^R), a temperature sensitive origin of replication, and the Cre recombinase gene under the control of the tetracycline-responsive promoter, was introduced into the zeocin-resistant bacteria by transformation. The bacteria were then cultured in LB media with tetracycline at 50 μg/ml for 3 h at 30°C to allow Cre expression and site-specific recombination between the two LoxP sites resulting in the excision of the Zeo^R. The tetracycline-resistant colonies were selected and verified for the presence of KSHV genome and removal of the Zeo^R. The Cre-expression plasmid was eliminated by culturing the bacteria at 42°C.

The revertant ΔmiRs_rt was generated in two steps using ΔmiRs as a template. First, two PCR products were generated. One product was obtained using primers 5’ATACTCGAGGTGTAGGCTGGAGCTGCTTC3’ and 5’GTATCTGATTTAATAAACACTAACAAGTTTTGTAAGAATCATTAGAATGCCAT

ATGAATATCCTCCTTAG3', and pMS102-Zeocin as a template. This fragment contained the Zeo^R flanked by LoxP sites together with a fragment of 50 bp KSHV sequence (genome position: 122056–122106) at one end and an XhoI restriction site at the other end. A second product was obtained using primers
5'GACCCAGCTGGTTTCCATAAATGGATATACTTCCGGAAAACGAAGGAGGG3' and
5'ATACTCGAGGTGCTTCTGTTTGAAGGCGAATAAAACAGGAAGCGGGTTGGACTGGCAGGGT3', and BAC36 DNA as a template. This product contained the sequence of the entire miR cluster with an XhoI site at one end. Second, these two PCR products were ligated after XhoI digestion resulting in a cassette containing the miR cluster and Zeo^R, which was then electroporated into *E. coli* DH10 containing ΔmiRs. Selection of colonies containing KSHV genomes with the miR cluster repaired followed by excision of the Zeo^R led to the generation of ΔmiRs _rt.

Cell culture and virus induction

Human embryonic kidney 293T cells were cultured in Dulbecco's modified Eagle's medium with 10% of fetal bovine serum (FBS). For stable selection of cultures of recombinant viruses, hygromycin at 200 μg/ml was added to the media. KSHV-infected primary effusion lymphoma (PEL) BCP-1 cells20 were cultured in RPMI-1640 with 10% of FBS. To induce viral lytic replication, cells were treated with 20 ng/ml of TPA and 0.25 mM sodium butyrate (T/B) for the specified lengths of time. To determine virion production, supernatants from cells induced for 5 days were collected and filtered through 0.45 μm filters. Virions were pelleted by ultracentrifugation, treated sequentially by Turbo DNAase I (Ambion, Austin, TX), and proteinase K. Virion DNA was determined by quantitative real-time PCR (qPCR) following DNA extraction. Purified BAC36 DNA was used as a copy number control.

Quantitative real-time reverse transcription PCR (RT-qPCR)

Total RNA isolated with Trizol reagent (Invitrogen, Carlsbad, CA) was treated with DNase I. RT-qPCR for KSHV genes was carried out as previously described33. Real-time quantification of miRs was carried out by stem-loop RT-qPCR34. A reverse transcriptase reaction was first carried out by incubating the RNA sample with a stem-loop RT primer for 30 min at 16°C, 30 min at 42°C, 5 min at 85°C, and then held at 4°C. qPCR was performed on a 7700HT Sequence Detection System (Applied Biosystems, Foster City, CA). The reactions were carried out in a 96-well plate at 95°C for 10 min, followed by 40 cycles at 95°C for 15 s, and then 60°C for 1 min. All the reactions were run in triplicates. The differences of cycle threshold values (C_T) between the samples (ΔC_T) were calculated after calibration with GAPDH and converted to fold changes using one of the samples as a standard (1-fold). The primers used in RT-qPCR are listed in Supplementary Table 1.

Plasmids

KSHV RTA promoter-luciferase reporter plasmid was described previously35. NF-κB reporter plasmid, containing tandem repeats of consensus NF-κB binding sites, was obtained from Dr. Bill Sudgen. NF-κB DN plasmid pIκB-αM was kindly provided by Dr. Paul J.

Chiao. The construction of IκBα 3'UTR luciferase reporter plasmid IκBα3UTRluc (IκBα-WT) was carried out by inserting the full-length of IκBα 3'UTR sequence downstream of the luciferase sequence into the pGL3 vector. Deletions of the two putative miR-K1 binding sites S1 and S2 from IκBα 3'UTR were performed by site-directed mutagenesis using primers 5'GTGGTACATGTAACAGCCAGGAGTGTTAAGCGTTC3' and 5'TACATGTACCACTGGGGTCAGTCACTCGAAGC3' for site 1, and primers 5'GTTACCCATGGTGTACATAATGTATTGTTGG3', 5'TACACCATGGGTAACACAAACCTTGACAGG3' for site 2 (Fig. 3i). Corresponding reporters were named IκBα3UTRlucΔS1 (ΔS1), IκBα3UTRlucΔS2 (ΔS2), IκBα3UTRlucΔS1+2 (ΔS1+2), respectively. Reporters containing different numbers of tandem repeats of the miR-K1 binding sites were generated by fusing the repeats through Hind III sites and cloning the products into the pGL3 vector. To construct 3'UTR luciferase reporter plasmids of RTA and ZTA type I, II and III transcripts16, we inserted their full-length 3'UTR sequences into the pGL3 vector downstream of the luciferase sequence between KpnI and XhoI sites after PCR amplification of cDNAs with the following primers RTA3'UTR-KpnI-F: 5'TTTTGGTACCAGTGTTCGCAAGGGCGTCTGTGCCT3' and RTA3'UTR-XhoI-R: 5'TCTC CTCGAGGTAGGGTTTCTTACGCCGGCATCGT3'. Sequences of RTA and ZTA transcripts were based on AF091348, AF091349 and AF091350. To express the miR cluster or individual KSHV miRs, the whole cluster or individual miR fragments were cloned by PCR amplification as previously described36, and inserted between BglII and HindIII sites of an expression vector pSUPER.retro.puro (OligoEngine, Seattle, WA). The sensor plasmids for KSHV miRs containing two repeats of perfect matching sequences of the respective miRs were described previously36.

Reporter assays

The luciferase reporter constructs and β-galactosidase expression plasmid pSV-β-gal (Promega, Madison, WI) were cotransfected into cells cultured in 24-well plates using the F2 transfection reagent (Targeting Systems, El Cajon, CA). For induction, cells transfected for 24 h were treated with T/B for 12 h. Other reporter assays were performed with the indicated expression plasmids and lengths of transfection time. Cells were then lysed, and the luciferase and β-gal activities were measured using luciferase and β-galactosidase kits (Promega). Luciferase activity was normalized to β-galactosidase activity. Results were calculated as means ± SEM from at least three independent experiments, each in triplicates except Fig 4a, which the means were calculated from two independent experiments, each in triplicates.

Western-blotting

Protein samples were separated by sodium dodecyl sulfate-polyacrylamide gel electrophoresis and transferred onto nitrocellulose membranes as previously described37. The membranes were first blocked with 5% non-fat milk and then incubated with a primary antibody followed with a horseradish peroxidase (HRP)-conjugated secondary antibody (Sigma, Life Science, St. Louis, MO). Specific bands were revealed with chemiluminescence substrates (Roche, Nutley, NJ) and recorded with an IS2000MM Imaging Scanner (Eastman Kodak Company, Rochester, NY). Antibodies to the following

proteins were used: IKKα, IKKβ, IKKγ, IκBα, IκBβ, and IκBε, all from GeneTex (San Antonio, TX), and β-tubulin (Sigma).

Immunofluorescence assay (IFA)

Cells grown on cover slid were first fixed with methanol or 1% paraformaldehyde, and blocked with 10% FBS. Cells were then incubated with primary antibody, and specific signal was detected with a secondary antibody conjugated with Alexa Fluor 568 (Invitrogen). The cells were counter-stained with 4', 6'-diamidino-2-phenylindole (DAPI). Images were observed and recorded with a Zeiss Axiovert 200 M epifluorescence microscope (Carl Zeiss, Inc., Thornwood, NY). Antibodies to p65, p50 and cRel (Calbiochem, Gibbstown, NJ), ORF59 (a gift of Dr. Bala Chandran), and LANA (ABI, New York, NY) were used.

Electrophoretic mobility shift assay (EMSA)

Nuclear extracts were prepared as previously described35. Annealed double-stranded oligonucleotides containing a NF-κB consensus site (5'AGTTGAGGGACTTTCCTT3') were labeled with [γ-^{32}p]ATP. For gel shift assay, 4 μg of the nuclear extract was incubated for 20 min with 5×10^5 cpm of labeled probe in 20 μl of binding buffer containing 10 mM Tris-HCl at pH 7.6, 50 mM NaCl, 1 mM EDTA, 1 mM dithiothreitol, 5% glycerol, 1 μg/μl bovine serum albumin, and 2 μg of poly(dI-dC). A competition reaction was carried out in the same manner except that the mixture was pre-incubated with excess cold probe or an irrelevant oligonucleotide for 10 min before the addition of labeled probe. To detect NF-κB complexes, a supershift assay was carried out by adding 1 μg of a specific antibody to p65, p50, or c-Rel to the reaction followed by an additional 15 min of incubation. Corresponding IgG from a normal animal was used as a control. The reaction mixtures were separated in 6% polyacrylamide gels.

Northern-blot hybridization

Total RNA was fractionated on a 1% formaldehyde agarose gel, transferred to nylon membranes, and hybridized with 32P-labeled riboprobes of Pan and ORF5738.

miR-K1 suppressor

We inhibited the functions of miRs using locked nucleic acids (LNAs)/DNA-mixed oligonucleotides complementary to the miR sequences (miR suppressors). An antisense oligonucleotide containing LNAs forms highly specific and stable duplexes with the complementary RNA. When bound to a miR, the oligonucleotide prevents it from interacting with the RISC protein complex and its target39. Oligonucleotide suppressors for miR-K1 (5'GCTTACACCCAGTTTCCTGTAAT3'), -K3 (5'CGCTGCCGTCCTCAGAATGTGA3') and -K8 (5'CGTGCTCTCTCAGTCGCGCCTA3'), and a scrambled control (5'CATTAATGTCGGACAACTCAAT3'), all containing LNAs at eight consecutive centrally located bases (underlined) were designed39 and synthesized (Sigma). To suppress the function of a miR, 10 nM of the LNA oligonucleotide were transfected into BCP-1 cells using the siPORT NeoFX kit (Applied Biosystems).

Supplementary Material

Refer to Web version on PubMed Central for supplementary material.

ACKNOWLEDGMENTS

We thank Kenneth Izumi and Anthony Griffiths for their valuable suggestions. This work was supported by grants from American Cancer Society (#RSG-04-195) and National Institute of Health (CA096512, CA124332, CA132637 and DE017333) to S-J Gao. C. G. Kim was supported by Konkuk University in 2008.

REFERNCES

1. Ganem D. KSHV infection and the pathogenesis of Kaposi's sarcoma. Annu. Rev. Pathol. 2006; 1:273–296. [PubMed: 18039116]
2. Cai X, et al. Kaposi's sarcoma-associated herpesvirus expresses an array of viral microRNAs in latently infected cells. Proc. Natl. Acad. Sci. USA. 2005; 102:5570–5575. [PubMed: 15800047]
3. Pfeffer S, et al. Identification of microRNAs of the herpesvirus family. Nat. Methods. 2005; 2:269–276. [PubMed: 15782219]
4. Samols MA, Hu J, Skalsky RL, Renne R. Cloning and identification of a microRNA cluster within the latency-associated region of Kaposi's sarcoma-associated herpesvirus. J. Virol. 2005; 79:9301–9305. [PubMed: 15994824]
5. Grundhoff A, Sullivan CS, Ganem D. A combined computational and microarray-based approach identifies novel microRNAs encoded by human gamma-herpesviruses. Rna. 2006; 12:733–750. [PubMed: 16540699]
6. O'Hara AJ, et al. Pre-microRNA signatures delineate stages of endothelial cell transformation in Kaposi's sarcoma. PLoS Pathog. 2009; 5 e1000389.
7. Gottwein E, et al. A viral microRNA functions as an orthologue of cellular miR-155. Nature. 2007; 450:1096–1099. [PubMed: 18075594]
8. Skalsky RL, et al. Kaposi's sarcoma-associated herpesvirus encodes an ortholog of miR-155. J. Virol. 2007; 81:12836–12845. [PubMed: 17881434]
9. Samols MA, et al. Identification of cellular genes targeted by KSHV-encoded microRNAs. PLoS Pathog. 2007; 3:e65. [PubMed: 17500590]
10. Ziegelbauer JM, Sullivan CS, Ganem D. Tandem array-based expression screens identify host mRNA targets of virus-encoded microRNAs. Nat. Genet. 2009; 41:130–134. [PubMed: 19098914]
11. Nachmani D, Stern-Ginossar N, Sarid R, Mandelboim O. Diverse herpesvirus microRNAs target the stress-induced immune ligand MICB to escape recognition by natural killer cells. Cell Host Microbe. 2009; 5:376–385. [PubMed: 19380116]
12. Qin Z, Kearney P, Plaisance K, Parsons CH. Pivotal Advance: Kaposi's sarcoma-associated herpesvirus (KSHV)-encoded microRNA specifically induce IL-6 and IL-10 secretion by macrophages and monocytes. J. Leukoc. Biol. 2009
13. Zhou FC, et al. Efficient infection by a recombinant Kaposi's sarcoma-associated herpesvirus cloned in a bacterial artificial chromosome: application for genetic analysis. J. Virol. 2002; 76:6185–6196. [PubMed: 12021352]
14. Greene W, et al. Molecular biology of KSHV in relation to AIDS-associated oncogenesis. Cancer Treat. Res. 2007; 133:69–127. [PubMed: 17672038]
15. Murphy E, Vanicek J, Robins H, Shenk T, Levine AJ. Suppression of immediate-early viral gene expression by herpesvirus-coded microRNAs: implications for latency. Proc. Natl. Acad. Sci. USA. 2008; 105:5453–5458. [PubMed: 18378902]
16. Zhu FX, Cusano T, Yuan Y. Identification of the immediate-early transcripts of Kaposi's sarcoma-associated herpesvirus. J. Virol. 1999; 73:5556–5567. [PubMed: 10364304]
17. Ye FC, et al. Kaposi's sarcoma-associated herpesvirus latent gene vFLIP inhibits viral lytic replication through NF-kappaB-mediated suppression of the AP-1 pathway: a novel mechanism of virus control of latency. J. Virol. 2008; 82:4235–4249. [PubMed: 18305042]

18. Nelson DE, et al. Oscillations in NF-kappaB signaling control the dynamics of gene expression. Science. 2004; 306:704–708. [PubMed: 15499023]
19. Ashall L, et al. Pulsatile stimulation determines timing and specificity of NF-kappaB-dependent transcription. Science. 2009; 324:242–246. [PubMed: 19359585]
20. Gao SJ, et al. KSHV antibodies among Americans, Italians and Ugandans with and without Kaposi's sarcoma. Nat. Med. 1996; 2:925–928. [PubMed: 8705864]
21. Lewis BP, Burge CB, Bartel DP. Conserved seed pairing, often flanked by adenosines, indicates that thousands of human genes are microRNA targets. Cell. 2005; 120:15–20. [PubMed: 15652477]
22. John B, et al. Human MicroRNA targets. PLoS Biol. 2004; 2:e363. [PubMed: 15502875]
23. Stern-Ginossar N, et al. Host immune system gene targeting by a viral miRNA. Science. 2007; 317:376–381. [PubMed: 17641203]
24. Grey F, Meyers H, White EA, Spector DH, Nelson J. A human cytomegalovirus-encoded microRNA regulates expression of multiple viral genes involved in replication. PLoS Pathog. 2007; 3:e163. [PubMed: 17983268]
25. Barth S, et al. Epstein-Barr virus-encoded microRNA miR-BART2 down-regulates the viral DNA polymerase BALF5. Nucleic Acids Res. 2008; 36:666–675. [PubMed: 18073197]
26. Umbach JL, et al. MicroRNAs expressed by herpes simplex virus 1 during latent infection regulate viral mRNAs. Nature. 2008
27. Ye FC, et al. Disruption of Kaposi's sarcoma-associated herpesvirus latent nuclear antigen leads to abortive episome persistence. J. Virol. 2004; 78:11121–11129. [PubMed: 15452232]
28. Li QH, Zhou FC, Ye FC, Gao SJ. Genetic disruption of KSHV major latent nuclear antigen LANA enhances viral lytic transcriptional program. Virology. 2008; 379:234–244. [PubMed: 18684478]
29. Karin M. NF-kappaB and cancer: mechanisms and targets. Mol. Carcinog. 2006; 45:355–361. [PubMed: 16673382]
30. Chaudhary PM, Jasmin A, Eby MT, Hood L. Modulation of the NF-kappa B pathway by virally encoded death effector domains-containing proteins. Oncogene. 1999; 18:5738–5746. [PubMed: 10523854]
31. Matta H, Chaudhary PM. Activation of alternative NF-kappa B pathway by human herpes virus 8-encoded Fas-associated death domain-like IL-1 beta-converting enzyme inhibitory protein (vFLIP). Proc. Natl. Acad. Sci. USA. 2004; 101:9399–9404. [PubMed: 15190178]
32. Mitchell T, Sugden B. Stimulation of NF-kappa B-mediated transcription by mutant derivatives of the latent membrane protein of Epstein-Barr virus. J. Virol. 1995; 69:2968–2976. [PubMed: 7707523]
33. Yoo SM, Zhou FC, Ye FC, Pan HY, Gao SJ. Early and sustained expression of latent and host modulating genes in coordinated transcriptional program of KSHV productive primary infection of human primary endothelial cells. Virology. 2005; 343:47–64. [PubMed: 16154170]
34. Chen C, et al. Real-time quantification of microRNAs by stem-loop RT-PCR. Nucleic Acids Res. 2005; 33:e179. [PubMed: 16314309]
35. Xie JP, Ajibade AO, Ye FC, Kuhne K, Gao SJ. Reactivation of Kaposi's sarcoma-associated herpesvirus from latency requires MEK/ERK, JNK and p38 multiple mitogen-activated protein kinase pathways. Virology. 2008; 371:139–154. [PubMed: 17964626]
36. Gottwein E, Cai X, Cullen BR. A novel assay for viral microRNA function identifies a single nucleotide polymorphism that affects Drosha processing. J. Virol. 2006; 80:5321–5326. [PubMed: 16699012]
37. Gao SJ, et al. Seroconversion to antibodies against Kaposi's sarcoma-associated herpesvirus-related latent nuclear antigens before the development of Kaposi's sarcoma. N. Engl. J. Med. 1996; 335:233–241. [PubMed: 8657239]
38. Wang XP, et al. Characterization of the promoter region of the viral interferon regulatory factor encoded by Kaposi's sarcoma-associated herpesvirus. Oncogene. 2001; 20:523–530. [PubMed: 11313983]
39. Kurreck J, Wyszko E, Gillen C, Erdmann VA. Design of antisense oligonucleotides stabilized by locked nucleic acids. Nucleic Acids Res. 2002; 30:1911–1918. [PubMed: 11972327]

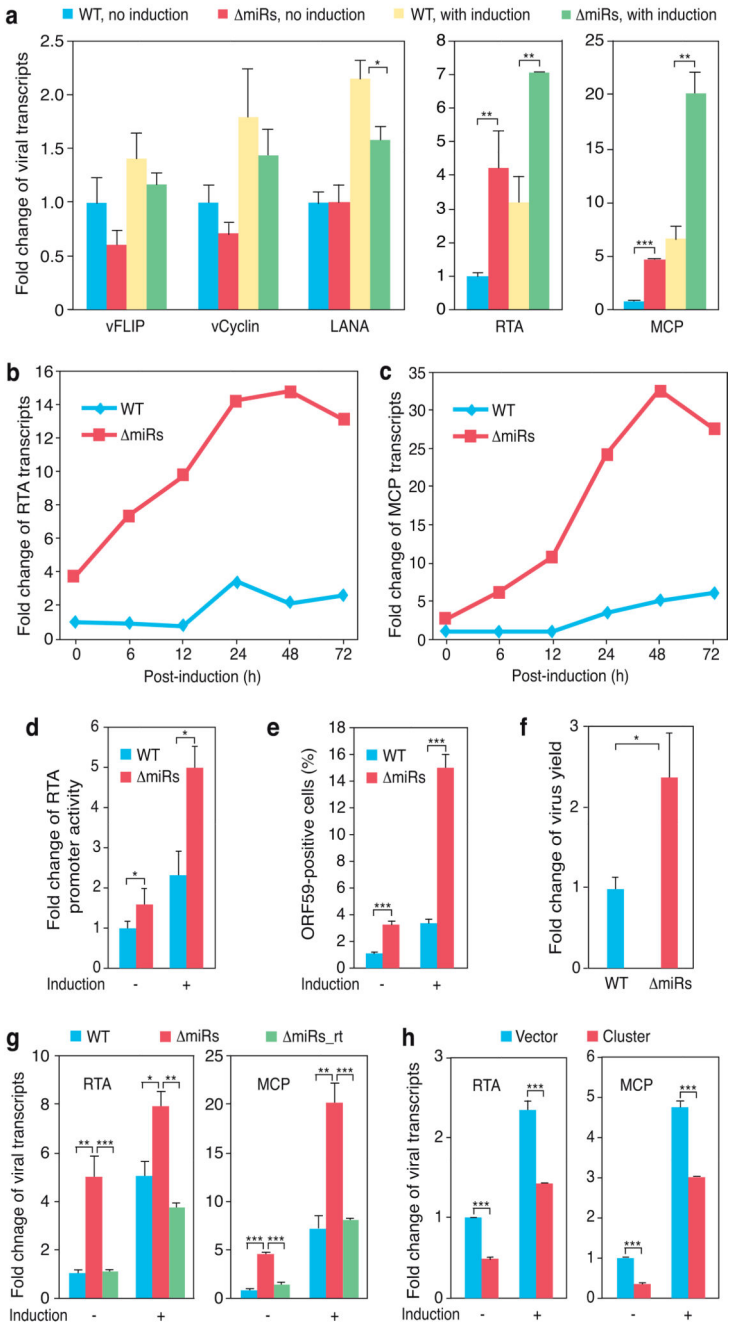

Figure 1.

KSHV miR cluster inhibits viral lytic replication. (**a**) Quantitative real-time reverse transcription PCR (RT-qPCR) analysis of KSHV latent genes (first panel) and lytic genes (second and third panels) in uninduced WT and ΔmiRs 293T cells, and cells induced for viral lytic replication with TPA and sodium butyrate (T/B) for 48 h. (**b**–**c**) Expression kinetics of KSHV lytic genes RTA (**b**) and MCP (**c**) in WT and ΔmiRs cells induced with T/B. (**d**) RTA promoter activity in uninduced and T/B-induced WT and ΔmiRs cells measured by a reporter assay. RTA promoter reporter construct was transfected into WT and

ΔmiRs cells for 36 h. Induced cells were treated with T/B for 6 h before cell collection. (**e**) Detection of ORF59 protein in uninduced WT and ΔmiRs cells, and cells induced with T/B for 48 h by immunofluorescence assay. (**f**) Relative virus yields of WT and ΔmiRs cells induced with T/B for 5 days. (**g**) RT-qPCR analysis of RTA and MCP transcripts in uninduced WT, ΔmiRs and ΔmiRs_rt cells, and cells induced with T/B for 48 h. (**h**) Levels of RTA and MCP transcripts examined by RT-qPCR in uninduced ΔmiRs cells stably transfected with a miR cluster expression vector, or cells induced with T/B for 48 h. Data are means ± SEM from three (**b**–**h**, n = 3) or five (**a**, n = 5) independent experiments. * $P<0.05$, ** $P<0.01$, *** $P<0.001$.

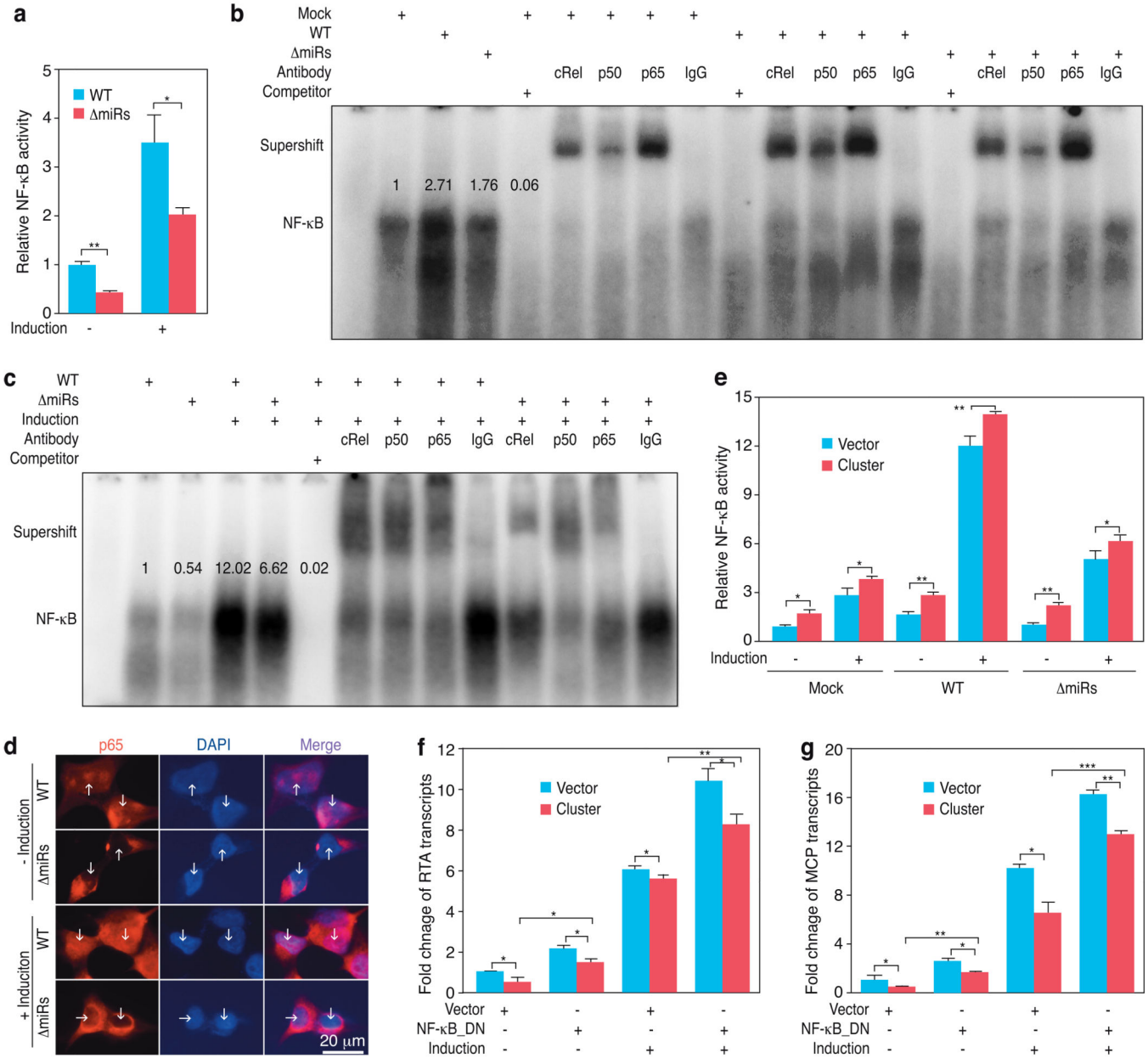

Figure 2.

KSHV miR cluster enhances NF-κB activity. (**a**) NF-κB reporter activities in WT and ΔmiRs 293T cells following transfection for 36 h. Induced cells were treated with TPA and sodium butyrate (T/B) for 6 h before cell collection. (**b**) NF-κB activities in uninfected mock, WT and ΔmiRs cells examined by electrophoretic mobility shift assay (EMSA). Unlabeled probe was used as a competitor. Antibodies to cRel, p50 and p65 were used to supershift the NF-κB DNA-protein complex. Image was from overnight exposure. Numbers on lanes are relative intensities. (**c**) NF-κB activities in uninduced WT and ΔmiRs cells, or cells induced with T/B for 24 h examined by EMSA as described in (**b**). Image was from 1 h exposure. (**d**) p65 staining by immunofluorescence assay in uninduced WT and ΔmiRs cells,

or cells induced with T/B for 24 h. WT cells had stronger p65 staining in nuclei identified by DAPI than ΔmiRs cells had (white arrow). (**e**) NF-κB reporter activities in uninfected mock, WT and ΔmiRs cells cotransfected with a miR cluster expression vector for 36 h. Induced cells were treated with T/B for 6 h before cell collection. (**f**–**g**) Levels of RTA (**f**) and MCP (**g**) transcripts examined by quantitative real-time reverse transcription PCR in ΔmiRs cells transfected with a miR cluster expression vector alone, or together with NF-κB dominant negative (DN) plasmid pIκB-αM for 72 h. T/B induction was carried out for 48 h before cell collection. Data are means ± SEM from three (**e**–**g**, n = 3) or four (**a**, n = 4) independent experiments. For image panels, representative images from two (**b**, **c**) and four (**d**) independent experiments are presented. * $P<0.05$, ** $P<0.01$, *** $P<0.001$.

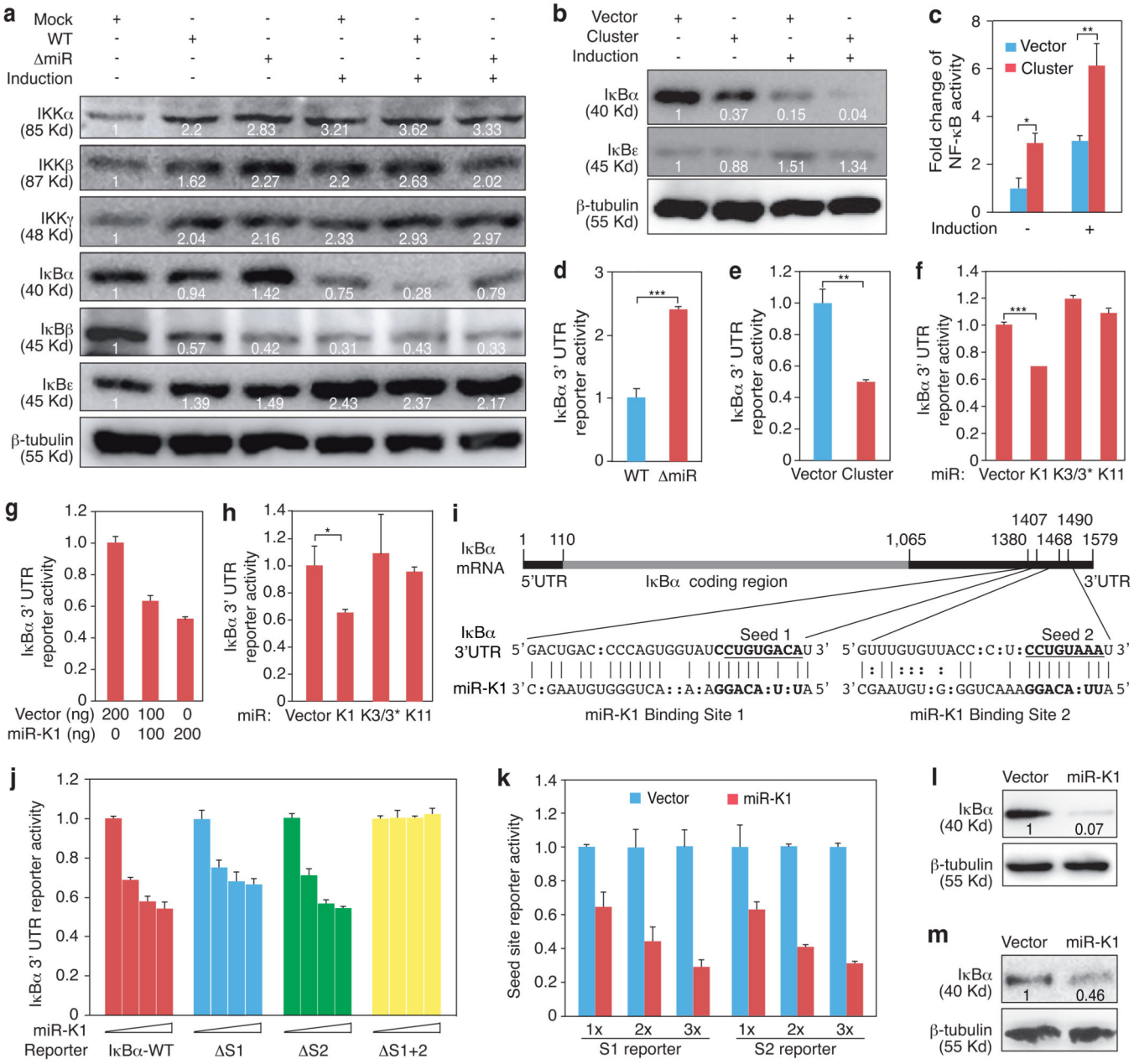

Figure 3.

KSHV miR cluster regulates NF-κB pathway through miR-K1 direct targeting of IκBα 3'UTR. (**a**) Levels of IKK and IκB proteins in uninduced mock, WT and ΔmiRs 293T cells, and cells induced with TPA and sodium butyrate (T/B) for 48 h. (**b**) IκBα and IκBε protein levels in BCP-1 cells transfected with a miR cluster expression vector for 96 h. T/B induction was carried out for 48 h before cell collection. (**c**) NF-κB reporter activities in BCP-1 cells cotransfected with a miR cluster expression vector for 36 h. T/B induction was carried out for 6 h before cell collection. (**d**) IκBα 3'UTR reporter (IκBα-WT) activities in WT and ΔmiRs 293T cells following transfection for 36 h. (**e**) IκBα-WT reporter activities in ΔmiRs 293T cells cotransfected with a miR cluster expression vector for 36 h. (**f**) IκBα-

WT reporter activities in 293T cells cotransfected with an expression vector of miR-K1, -K3/3*, or -K11 for 36 h. (**g**) IκBα-WT reporter activities in 293T cells cotransfected with increasing doses of miR-K1 expression vector for 36 h. (**h**) IκBα-WT reporter activities in ΔmiRs 293T cells cotransfected with an expression vector of miR-K1, -K3/3*, or -K11 for 36 h. (i) Structure of IκBα transcript, its 3'UTR, and two putative miR-K1 binding sites (S1 and S2). (**j**) Reporter activity of IκBα-WT or mutant construct with either S1 (ΔS1), S2 (ΔS2) or both sites (ΔS1+2) mutated following cotransfection with a miR-K1 expression vector at increasing doses (0, 100, 200 and 400 ng) for 36 h. (**k**) Activities of reporters with 1 to 3 repeats of targeting sites following cotransfection with a miR-K1 expression vector for 36 h. (**l**–**m**) IκBα protein levels in KSHV-negative (**l**) or ΔmiRs 293T cells (**m**) transfected with a miR-K1 expression vector for 96 h. Data are means ± SEM from three (**c**, **d**, **g**, **h**, **j**, **k**, n = 3) or four (**e**, **f**, n = 4) independent experiments. For image panels, representative images from two (**b**), three (**a**) and four (**l**, **m**) independent experiments are presented. Numbers labeled on the lanes are relative intensities of the bands. * $P<0.05$, ** $P<0.01$, *** $P<0.001$.

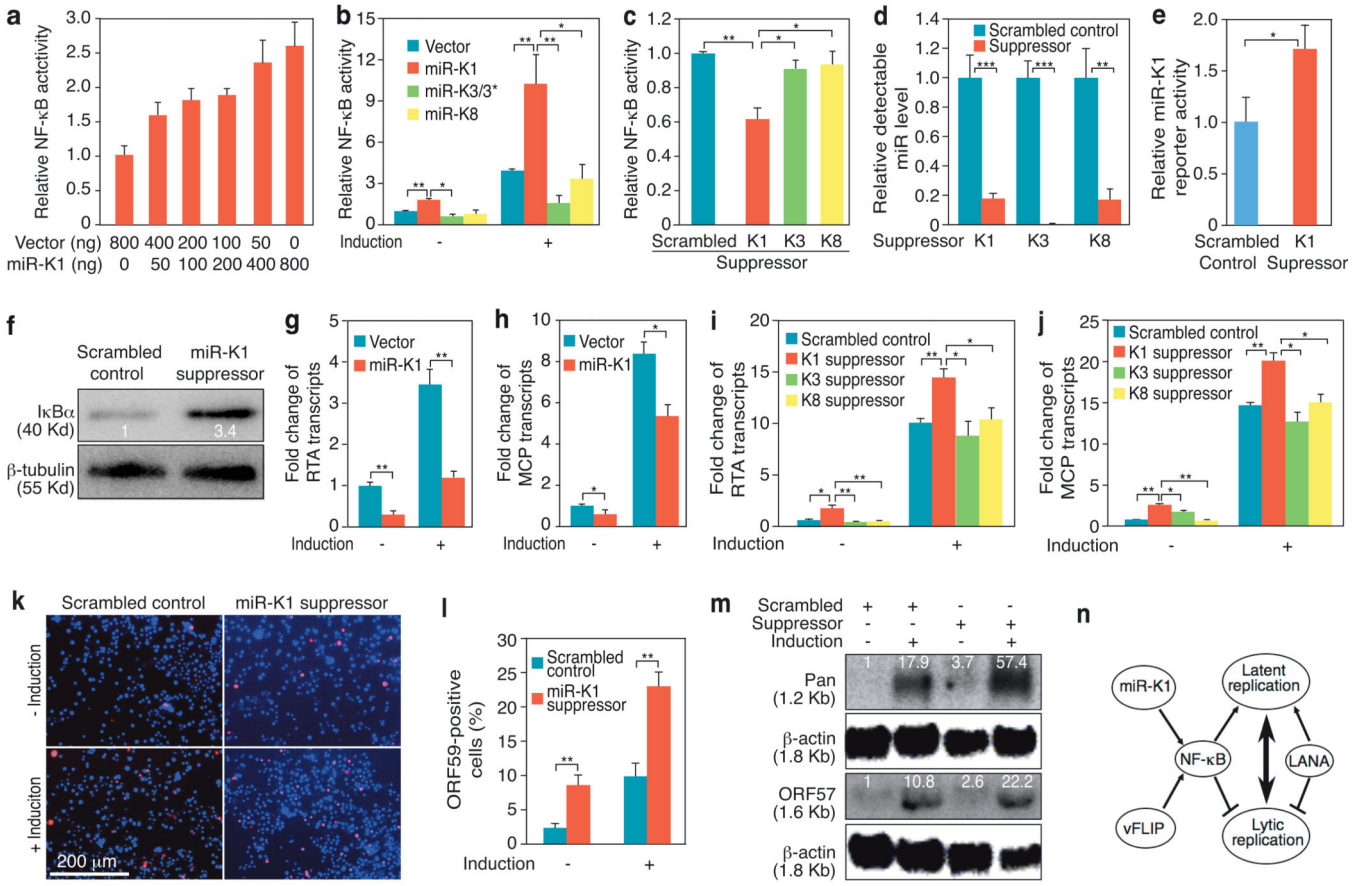

Figure 4.

KSHV miR-K1 inhibits viral lytic replication by enhancing NF-κB activity. (**a**) NF-κB reporter activities in 293T cells cotransfected with increasing doses of miR-K1 expression vector for 48 h. (**b**) NF-κB reporter activities in ΔmiRs 293T cells cotransfected with miR-K1, -K3/3*, or -K8 for 48 h. TPA and sodium butyrate (T/B) treatment was carried out for 24 h before cell collection. (**c**) NF-κB reporter activities in PEL cells transfected with a suppressor of miR-K1, -K3 or -K8 for 48 h followed by transfection of a NF-κB reporter construct for another 24 h. (**d**) Levels of miRs measured by quantitative real-time reverse transcription PCR (RT-qPCR) in BCP-1 cells transfected with a suppressor of miR-K1, -K3 or -K8 for 48 h. (**e**) miR-K1 sensor reporter activities in WT cells cotransfected with miR-K1 suppressor for 48 h. (**f**) IκBα protein levels in BCP-1 cells transfected with miR-K1 suppressor for 48 h. Numbers on lanes are relative intensities. (**g**–**h**) Levels of RTA and MCP transcripts determined by RT-qPCR in uninduced ΔmiRs cells stably transfected with a miR-K1 expression vector, or cells induced with T/B for 48 h. (**i**–**j**) Levels of RTA and MCP transcripts determined by RT-qPCR in BCP-1 cells transfected with a suppressor of miR-K1, -K3 or -K8 for 72 h. T/B induction was carried out for 48 h before cell collection. (**k**) Expression of ORF59 protein examined by immunofluorescence staining in BCP-1 cells transfected with miR-K1 suppressor for 72 h. Induced cells were treated with T/B for 48 h. (**l**) Statistical results of panel **k**. (**m**) Levels of Pan and ORF57 transcripts examined by Northern hybridization in BCP-1 cells transfected with miR-K1 suppressor for 72 h. Induced

cells were treated with T/B for 48 h. Numbers on lanes are relative intensities. (**n**) A model of KSHV latency and replication regulated by miR-K1 and latent genes. Data are means ± SEM from three (**c**–**e**, **g**–**j**, n = 3) or four (**b**, **l**, n = 4) independent experiments. For panel **a**, the results are means from two independent experiments. For image panels, representative images from two (**f**, **m**) and four (**k**) independent experiments are presented. * $P<0.05$, ** $P<0.01$, *** $P<0.001$.